Deciphering the complex paramagnetic NMR spectra of small laccase

Dasgupta, R.

Chapter 2

Chemical exchange at the tri-nuclear copper center of small laccase from *Streptomyces coelicolor*

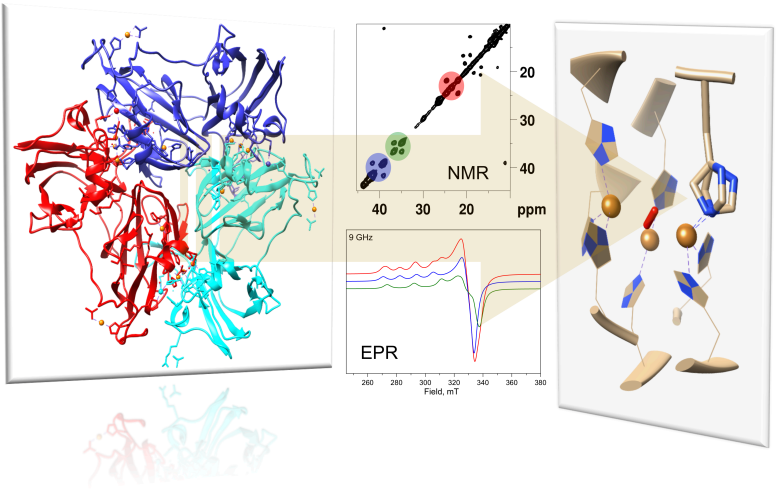

This chapter is published as:
Dasgupta, R., K.B.S.S. Gupta, F. Nami, H.J.M. de Groot, G.W. Canters, E.J.J. Groenen, and M. Ubbink. 2020. Chemical exchange at the trinuclear copper center of small laccase from *Streptomyces coelicolor*. *Biophysical Journal*. 119:9–14. DOI: http://doi.org/10.1016/j.bpj.2020.05.022

EPR spectroscopy was performed and the data were analyzed by F. Nami, G. W. Canters and E. J. J. Groenen.

The tri-nuclear copper center (TNC) of laccase reduces oxygen to water with very little overpotential. The arrangement of the coppers and ligands in the TNC is known from many crystal structures, yet information about possible dynamics of the ligands is absent. Here, we report dynamics at the TNC of small laccase from *S. coelicolor* using paramagnetic NMR and EPR spectroscopy. Fermi contact-shifted resonances tentatively assigned to histidine Hδ1, display two-state chemical exchange with exchange rates in the order of 100 s^{-1}. In the EPR spectra, at least two forms are observed with different g_z values. It is proposed that the exchange processes reflect rotational motion of histidine imidazole rings that coordinate the coppers in the TNC.

2.1 Introduction

Laccases reduce dioxygen to two water molecules at the tri-nuclear copper center (TNC) by oxidizing a broad range of substrates at the type 1 (T1) site, with very little overpotential,(1) making them potentially interesting proteins for enzymatic biofuel cells. The TNC (Figure 2.1d and 1.4a) comprises a type 3 (T3) site with two coppers and a type 2 (T2) site with a single copper. The T1 site is linked to the TNC via a conserved HCH motif and the two are separated by ~ 13 Å (Figure 1.3). This conserved motif provides a fast route for electron transfer from the substrate via the T1 site to the TNC for O_2 reduction to water. Crystal structures of laccases (2–8) have helped in modelling the catalytic mechanism of O_2 reduction.(2, 4) The current model for the catalytic mechanism for O_2 reduction at the TNC is summarized in Chapter 1 (Figure 1.3). In brief, the resting oxidized (RO) state is converted to fully reduced (FR) state by receiving four electrons from substrate oxidized at the T1 site. The FR state can bind oxygen and is converted to peroxide intermediate (PI) state by transferring 2 electrons to the oxygen molecule hence forming a peroxide. The PI state is converted to native intermediate (NI) state, in which the oxygen bond has been cleaved and all the coppers in the TNC are coupled via an oxygen atom. This NI state can slowly be converted to RO state in the absence of the substrate or directly go into the FR state in the presence of the substrate.(2–4)

Although much is known about the mechanism through different models, mimicking the active site to design artificial catalyst is notoriously difficult. The model compounds reported so far do not have the catalytic efficiency of the enzyme.(9–12) Usually dynamics associated with the residues at the active site is ignored while designing artificial catalyst although it was reported that motions can be important to attain a conformation that lowers the energy barrier for electron and proton transfer processes.(13–16) Determining such motions in laccase might provide insight into designing a functional framework for an efficient artificial catalyst. Here, we report

the presence of conformational exchange at the TNC on the millisecond timescale, ascribed to motions of the copper coordinating imidazole rings of histidine residues.

2.2 Results and discussions

A mutant of small laccase from *S. coelicolor* (SLAC) was used, in which the T1 site is copper depleted by the C288S mutation (SLAC-T1D).(8) The theoretical MW of the holoenzyme in its monomeric form is 37.05 kDa. The purified protein was found to run at an apparent MW of 75 kDa and 37 kDa in SDS PAGE (Figure S2.1) but in solution it has a MW ~ 105 kDa, as determined by size exclusion chromatography linked with multi angle light scattering (SEC-MALS). Thus, it is concluded that the enzyme is in its trimer form, as observed in crystal structure.(17)

Identification of nitrogen attached protons

The 1D ^{1}H WEFT-NMR (18) experiment enhances signals of protons experiencing rapid paramagnetic relaxation. The resulting NI state spectrum of SLAC-T1D (Figure 2.1a) shows large Fermi contact shifts (FCS) (> 21 ppm) for many resonances. The spectrum is very similar to the one reported by Machczynski *et al.*, (2004 and 2016) (6, 19) confirming that TNC is fully formed. Fermi contact interactions fall off rapidly with the number of bonds between metal and nucleus,(20) indicating that the resonances with large shifts must derive from sidechains of the copper coordinating amino acid residues, which are histidine ligands.(21, 22) Since the anisotropy of the copper sites in proteins is reported to be low,(20) the contribution of pseudo-contact shifts (PCS) to the observed chemical shift is much smaller than that of the FCS, though not necessarily negligible in all cases (maximal PCS estimations are provided in Table S2.5 using equation 1.11).

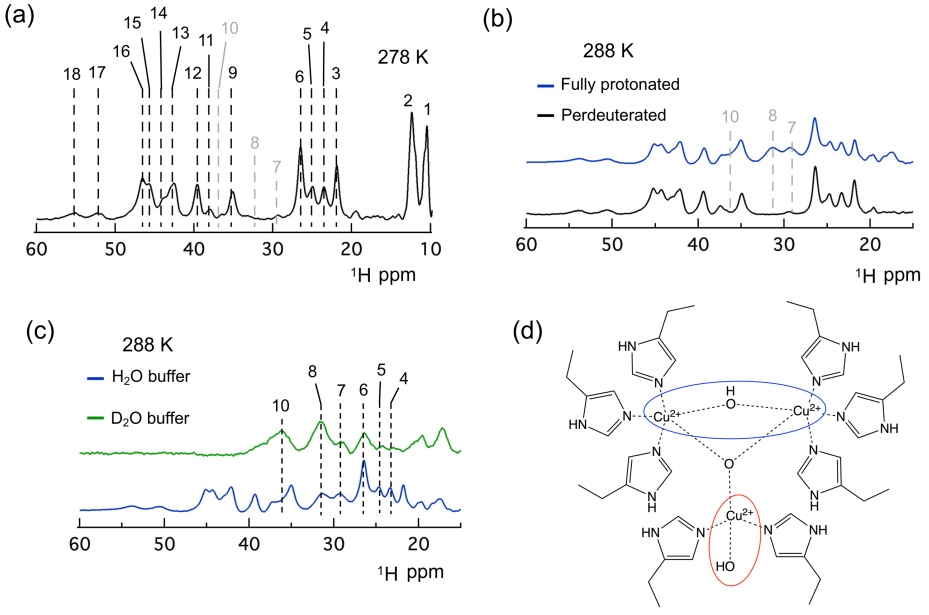

***Figure 2.1**. Analysis of the 1D ¹H spectra. (a) WEFT NMR spectra of perdeuterated protein with amide proton back-exchanged at 278 K depicting the part of the spectrum showing signals that are strongly shifted by Fermi contact effects. The resonance 7, 8 and 10 are indicated to shows their positions from panel b and c; (b) 1D WEFT spectra at 288 K comparing samples that were fully protonated (blue) or perdeuterated with back-exchange (black), both in H_2O buffer. Resonances 7, 8 and 10 are indicated which are derived from protons attached to carbons; (c) 1D WEFT spectra at 288 K comparing fully protonated samples in D_2O buffer (green) and H_2O buffer (blue), showing the extensive loss of resonances due to exchange of protons by deuterons and (d) Schematic representation of a tri-nuclear copper center of small laccase in the NI state. The T3 and T2 sites are marked by blue and red ovals. Hδ1 His ring protons are shown.*

Utilizing different deuteration schemes, resonances from protons attached to nitrogen/oxygen atoms can be distinguished from those attached to carbon, being exchangeable and non-exchangeable, respectively. For a per-deuterated sample that was allowed to back-exchange the exchangeable deuterons to protons, resonances 7 and 8 were lost from the spectrum, indicating that they derive from non-exchangeable, carbon-attached protons. The remaining resonances appear in the spectrum of this sample, indicating that they are from exchangeable protons, most likely attached to nitrogen atoms (Figure 2.1b). A normal, protonated sample in which exchangeable protons were replaced with deuterons by bringing the sample in D_2O yields a spectrum in which resonances 7, 8 and 10 are prominent, supporting the observation that the equivalent protons are attached to carbons (Figure 2.1c). For resonances 4, 5 and 6

(Figure 2.1a and c) the assignment is less clear, they may represent overlapping signals from exchangeable and non-exchangeable protons (Figure 2.1b, c).

Chemical exchange at the TNC

To probe the dynamics at the TNC, $^1H - ^1H$ exchange spectroscopy (EXSY) (23) was used with solvent pre-saturation during interscan delay (Figure 1.5b). We observe multiple cross peaks between the FCS resonances (> 22 ppm, Figure S2.2). NOE and exchange cross peaks were distinguished by comparing the temperature dependence of the cross-peak intensities, normalized by the diagonal peak intensities. For the temperature range used in the present work (278 – 303 K) NOE cross peak intensity will be independent with respect to temperature, while the EXSY cross peak intensity will show an increase with increasing temperature (Figure S2.2 and Figure 2.2a and b).(20) The cross peaks between resonances 3 & 5, 9 & 11, and 12 & 13 arise from chemical exchange, whereas the cross peak between resonance 12 and a resonance at 11 ppm is a NOE cross peak (Figure S2.2). Resonances between 27 and 30 ppm belong to protons attached to carbon atoms (Figure 2.1a, b and c). Cross-peaks were also observed between resonance pairs of 18-16 and 17-15 at very short mixing times of 1 ms and 2 ms and at 303 K (Figure S2.4). Cross peaks are also observed between the resonances in the spectra region from 11 to 22 ppm (Figure S2.5). However, due to the low S/N it could not be established whether these cross peaks are due to chemical exchange or NOE.

Table 2.1. *Kinetic parameters and equilibrium constants. The values [*] were obtained from the best fit (Figure S2.3) of the cross peak and diagonal intensities of the resonance pairs 3-5, 9-11 and 13-12 to equation S2.1. The rate constants k_A and k_B are the forward and reverse rates and k_{ex} is the total exchange rate ($k_A + k_B$). K_{eq} is the equilibrium constant obtained from the ratio of the diagonal peak integral volume at τ_{mix} = 0 ms and was constrained during fitting.*

Temp. (K)	3-5				9-11				13-12			
	(s^{-1})				(s^{-1})				(s^{-1})			
	k_A	k_B	k_{ex}	K_{eq}	k_A	k_B	k_{ex}	K_{eq}	k_A	k_B	k_{ex}	K_{eq}
293	34	45	79	0.76	48	61	109	0.78	15	29	44	0.52
298	33	62	95	0.53	29	91	120	0.32	29	34	63	0.85
303	46	81	127	0.56	48	127	175	0.37	22	44	66	0.50
308	68	115	183	0.59	81	160	241	0.50	36	48	84	0.75

[*] Error is estimated to be ~ ± 5% from duplicate measurements.

Thus, in the further analysis we focussed on the exchange peaks between resonances 3 – 5, 9 – 11 and 13 – 12. The chemical exchange is in the slow-exchange regime because a distinct resonance is observed for each state. The forward and backward chemical-exchange rates were determined for the three pairs of resonances using equations derived previously (equations S2.1 to S2.4, see also Figure S2.3).(24) Table 2.1 summarizes the exchange rates obtained from fittings of the ratio of the cross by diagonal peak intensities at different temperatures. The equilibrium constant is about 0.5 and does not change much in the applied temperature range, but the exchange rates increase about two-fold between 293 and 308 K for each resonance pair, allowing an estimation of the activation energy of the transition between the two states. The observed activation energies for the transitions of resonance 3 to 5, 9 to 11 and 13 to 12 are 43 ± 4 kJ/mol, 42 ± 7 kJ/mol and 30 ± 6 kJ/mol, respectively (Figure 2.2c).

Temperature dependence of proton chemical shift

Temperature dependence of the FCS resonances (Figure S2.10a) showed three types of behaviour, strong-Curie (decreasing hyperfine coupling with increasing temperature), for resonances 11, 13, 16, 15, 18 and 17, weak-anti-Curie (increasing hyperfine coupling with increasing temperature), for resonances 3, 6, 7 and 8, and no-Curie (temperature independent), for resonances 4, 5, 9 and 12, suggesting that there is more than one coupled copper pair, in line with previous reports.(19, 25) The quantitative analysis of the coupling scheme for the temperature dependence of the FCS resonances (Figure S2.10) is described in section 1.3 of Chapter 1. Using equation 1.4, the J coupling values were obtained from the temperature dependence of the FCS resonances, assuming a general triad ($J_{13} \neq J_{12} \neq J_{23}$ for NI form of SLAC-T1D, yielding $J_{12} = -120$ cm^{-1}, $J_{13} = -80$ cm^{-1} and $J_{23} = -150$ cm^{-1}, where J_{23} is the coupling between the T3 coppers (Figure S2.10b and c). The above values were obtained by procedure described in Machczynski *et al.*,(2016) (19) and it was observed that the values reported gave an excellent fit.

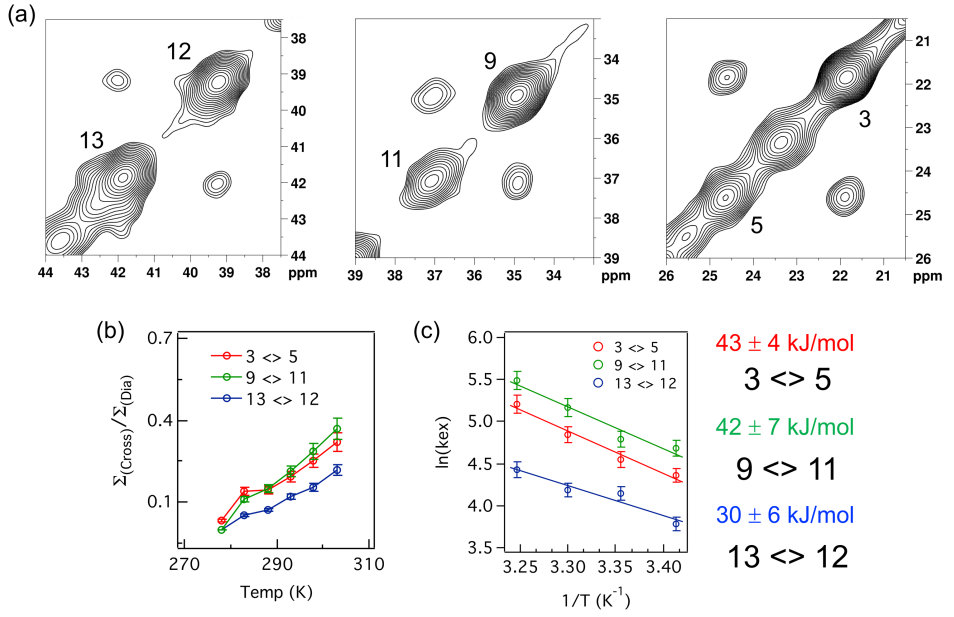

Figure 2.2. *Exchange effects. (a) 2D ^{1}H–^{1}H EXSY spectra of the region between > 22 ppm, showing resonances with exchange cross peaks. The spectrum was recorded at 288 K at 14.2 T (600 MHz). The numbering of resonances is equivalent to Figure 2.1a. (b) Temperature dependence of the sum of cross peak intensity, normalized with the sum of diagonal peak intensity of the resonances 3 – 5, 9 – 11 and 13 – 12 in red, green and blue, respectively. The error bars are calculated from the noise level. (c) Arrhenius plot and the respective activation energies for the exchange processes 3 ↔ 5, 9 ↔ 11 and 13 ↔ 12. The error is one standard deviation.*

Analysis of crystal structures

The FCS for the two states differ by ~ 3 ppm, a relatively small change for an absolute FCS in the order of 20-35 ppm, indicating a small change in the unpaired electron-spin density on the proton. In combination, these observations agree with an assignment of the resonances to the protons linked to the Nδ1 atoms of the imidazole rings of histidine ligands that coordinate the coppers in the T3 and T2 sites. Such protons are exchangeable with the solvent but the exchange is slow enough for the resonance to be observed because all but one Nδ1 atom in the TNC are hydrogen bonded (Table S2.3). These hydrogens will experience large FCS, being very close to the copper ions. A rearrangement of the imidazole ring, such as a small rotation, can leave the coordination intact, yet cause a slight change in spin density and thus in the FCS. An inspection of crystal structures of prokaryotic multicopper oxidases (3-domain monomeric laccases) yielded two examples (PDB: 3zx1 and 2xu9) (26, 27) in which imidazole ring motions at the T3 site were captured (Figure S2.6). In 3zx1 (resolution

1.95 Å) two conformations of the His-182 ring are observed with $\chi 2$ angles 154° and 86°, yet maintaining a coordination bond with the T3-Cu.(26) In structure 2xu9 (resolution 1.5 Å) the equivalent ligand, His-137, also displays two conformations, one of which has no coordination bond with T3-Cu.(27) In this case also the $\chi 1$ angle differs.

To estimate how much motion of the His rings could be accommodated at the TNC of SLAC, we modelled the change in distance between the T3-Cu and His Nε2 of the ligand His158, equivalent to His182.A in PDB 3zx1, as a function of the $\chi 2$ dihedral angle, using PDB 3cg8 (resolution 2.68 Å).(17) Allowing for a somewhat arbitrary maximal increase of 0.05 Å of the distance to maintain the coordination bond, avoiding clashes with surrounding atoms and maintaining the hydrogen bond of the Nδ1, the $\chi 2$ angle of His-158 can still assume values between 100° and 140° (Figure S2.6). Similar analysis was done for all the coordinating His at the TNC (Figure S2.7). In each case the imidazole ring has considerable freedom to rotate. An analysis of $\chi 2$ angles for a variety of 2-domain and 3-domain laccase structures reflects this freedom (Figure S2.8). This suggests that such ring motions might be responsible for the observed exchange behaviour. The detailed method is given in the supporting information.

Electron paramagnetic resonance spectroscopy

The NMR observations show the presence of at least 3 chemical exchange process at the TNC and we wondered whether one of it belongs to a ligand at the T2 site. If heterogeneity is present at the T2 site, distinct sites may show up in the EPR spectrum for the frozen protein. The low temperature EPR spectrum of SLAC-T1D yields a signal for the T2 site, while the coppers in the T3 site are anti-ferromagnetically coupled and thus EPR silent. The 9.5 GHz (X-band) spectrum at 40 K (Figure 2.3) reveals the copper hyperfine structure in the low-field part of the spectrum, the g_z region from 265 to 320 mT, be it not a simple pattern of four equidistant lines. In addition to the copper hyperfine structure, the spectrum shows a small but resolved hyperfine structure around 328 mT, which derives from the interaction of the copper electron spin with the nitrogen nuclear spins of the copper-coordinating histidine ligands. To interpret the X-band spectrum, we make use of the 275 GHz EPR spectrum taken at 10 K (Figure 2.3). At this high microwave frequency, the copper and nitrogen hyperfine structure is masked by line broadening due to *g*-strain. The higher *g*-resolution at this frequency clearly reveals two distinct signals in the g_z region, at 8.37 and 8.77 T, corresponding to $g_z = 2.352$ and $g_z = 2.246$. Starting from these values we simulated the EPR spectra at both microwave frequencies as the sum of the spectra of two components (Figure 2.3), which differ in the g_y, g_z, and A_z spin Hamiltonian parameters (Table S2.4). The separate contributions of the two components to the simulated spectra are shown in Figure S2.9. The parameters of the

major component 1 correspond to those previously reported for the T2 site of SLAC-T1D,(7) while the parameters of minor component 2 resemble those of the T2 site of multicopper oxidase from different organisms (Table S2.6 and references therein). The fraction of the minor component varies for different preparations, and is commonly between 30 and 40%. We believe that the distinct EPR signals for SLAC-T1D are evidence of heterogeneity in the T2 site of the TNC, in line with the observation of multiple states of the imidazole rings by NMR. The EPR spectrum at 275 GHz showing the difference in the value of g_z supports the presence of His ring motion at the T2 site, as a rearrangement/rotation of an imidazole ring will affect the delocalization of spin density between copper and the imidazole, thereby changing the spin density on the copper to which, through spin-orbit coupling, the g_z value is most sensitive.(28)

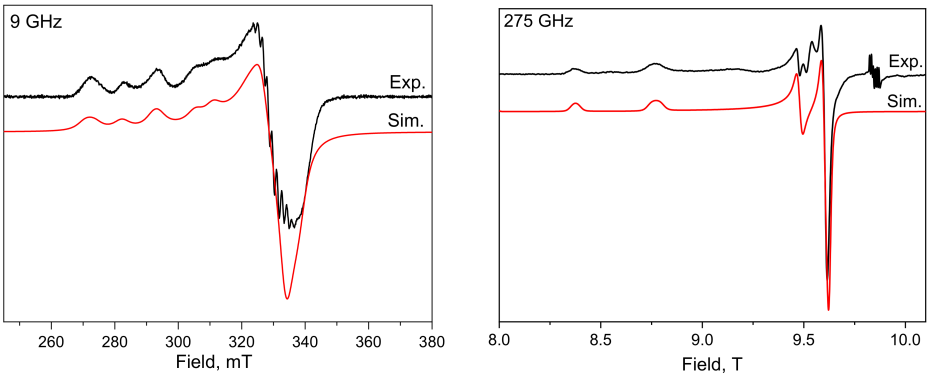

Figure 2.3. *Experimental and simulated EPR spectra of the resting form of SLAC-T1D (as purified) at microwave frequencies of 9.5 GHz and 275 GHz. The small signals around 9.85 T in the experimental spectrum at 275 GHz arise from a Mn (II) impurity in the sample. The hyperfine interaction of the copper electron spin with the nitrogen nuclei of the copper-coordinating histidine ligands is not considered for the simulations. The experimental and simulation details are summarized in supplementary material.*

2.3 Conclusion

NMR spectroscopy showed that at least 3 independent chemical exchange processes are present at the TNC and EPR spectroscopy showed that heterogeneity exists at the T2 site. We propose that in the NI state of SLAC there is chemical exchange at the TNC and this is due to the ring motions of coordinating histidine residues. The motions appear not to be concerted. Though the activation energies are similar within their error ranges, the exchange rates differ significantly (Table 2.1), indicating independent processes. Such motions could well be a general property of histidine rings, much like ring flips of aromatic residues. His ring flips in the influenza A M2 proton channel are associated with proton conduction, with an energy barrier greater than 59 kJ/mol.(29) A fast His flip (~2000 s^{-1}) was described in detail for the surface exposed, non-coordinating His61 in plastocyanin from *Anabaena variabilis*.(30) Here, the imidazole rings are not flipping (i.e. not rotating by 180°) because that would break the coordination bond, yet clearly two states exist, separated by a considerable activation barrier, perhaps representing two ring orientations with favourable coordination properties. It needs to be determined whether the same motions are present in wt SLAC. Given their local nature and the similarity in structures of T1D and wt laccases,(17, 19) it seems quite likely that also in wt SLAC such motions occur. Whether evolution has used His ring motions to the benefit of catalysis by SLAC, for example as a gatekeeper or for proton transfer, remains to be established.

2.4 Supporting Information

Production and purification of SLAC-T1D

SLAC-T1D was expressed and purified as described previously.(6, 8) Briefly, for fully protonated sample, pET20b plasmid containing the gene encoding SLAC C288S (type 1 depleted mutant) was transformed in BL21 pLysS strain of *Escherichia coli*. A colony of transformed cells was used to inoculate 25 mL lysogeny broth and the suspension was incubated overnight at 37°C. This preculture was diluted in 500 mL 2x YT medium, which was incubated at 30°C to an optical density at 600 nm of 1.0 to 1.5. Gene expression was induced with 0.5 mM IPTG. Then, the temperature was reduced to 25°C and cells were harvested after a further incubation during 18 hrs. For perdeuterated samples, the preculture was prepared in 25 mL of M9 minimal medium in water, which was transferred to 25 mL of M9 medium prepared in 99.99% D_2O for an overnight preculture. The latter was used to inoculate 500 mL D_2O-M9 minimal medium containing ^{15}N ammonium chloride and D-glucose-1,2,3,4,5,6,6-d7 as nitrogen and carbon sources respectively. Gene expression and protein harvesting was done as that of the fully protonated sample. Purification was done in 10 mM sodium phosphate buffer pH 7.3 (buffer A) for fully protonated and perdeuterated (with back-exchange of amide protons) samples.(6, 8) Briefly, the harvested cells were lysed with a French press in buffer A. After centrifugation, the soluble fraction was incubated with 1 mM $CuSO_4$ for 2-3 hrs at 4°C. Then, the soluble fraction was dialyzed against 5 L of buffer A for 18 hrs at 4°C. EDTA (1 mM) was added to the soluble fraction and dialyzed against 5 L of buffer A twice for 18 hrs at 4°C. The soluble fraction was pooled and loaded on a 10 ml DEAE column preequilibrated with buffer A and eluted with a gradient of 0-500 mM NaCl in buffer A in 40 column volumes. Fractions with green colour were pooled and concentrated using a Proteus X-spinner 10 kDa concentrator. For final purification the concentrated protein was loaded on a 120 mL Superdex 75 gel filtration column preequilibrated with buffer A with 150 mM NaCl. Green fractions were pooled, concentrated, buffer exchanged to buffer A at pH 6.8 and stored at -80°C after flash freezing for future use. The yield was 200 mg/L and 240 mg/L for fully protonated and perdeuterated samples respectively. After heating the samples at 95°C for 30s the purity was checked using 12.5% SDS PAGE gel, as shown in Figure. S2.1 where a band at ~ 37 kDa and ~ 75 kDa is observed belonging to monomer (M) and dimer (D) respectively. Under native condition from size exclusion chromatography with multi-angle light scattering (SEC-MALS) the molecular weight of the protein was ~ 105 kDa, which suggests the presence of a trimeric form.

NMR spectroscopy

Samples contained ~ 800 μM SLAC-T1D in 10 mM sodium phosphate buffer pH 6.8 with 10% D_2O for the samples that were fully protonated or perdeuterated with back-exchange. For samples in D_2O, the buffer was changed with a Proteus X-spinner 10 kDa concentrator to 10 mM sodium phosphate buffer pH 6.8 prepared in 99.99% D_2O. Experiments were done on a Bruker AV-III HD 600 MHz NMR spectrometer equipped with a TXI cryoprobe. 1D WEFT experiments were done with a WEFT delay and an interscan delay of 100 ms each (Figure 1.5a). Inversion recovery experiments to measure the spin-lattice relaxation rate were done using standard pulse sequence of d1–180–d2–90–acq where d1 is the interscan delay, which was set to 100 ms, d2 is the recovery time which was from 0.1 ms to 60 ms and acq is the acquisition. The intensity of the resonance vs the d2 time gives an exponential curve which was fitted with equation $I(t) = I(0)\left(1 - 2e^{(-t/T1)}\right)$, where $I(0)$ is the intensity at thermal equilibrium, t is the recovery time and T1 is the spin-lattice relaxation time. The inverse of the T1 relaxation time gives the spin-lattice relaxation rate and is summarized for the chemical exchange resonance pairs in Table S2.2. 2D ^{1}H-^{1}H EXSY(23, 31) experiments were recorded with an interscan delay of 200 ms and mixing times of 1, 2, 3.5, 5, 7 and 9 ms. For the study of the temperature dependence the samples were incubated at every temperature for 15 min. prior to data collection. The integral volume of cross peaks and diagonal peaks was obtained using TOPSPIN 4.0.5 (Bruker). The mixing time dependent integral volume profiles were fitted using equations S1-S4 (24) with IGOR Pro 6.3.7 to obtain the exchange rates. The fitting was done by constraining the K_{eq} (Table 2.1 of the main text) to the value of the ratio of the diagonal integral volume at zero mixing time.(24) The spin-lattice relaxation rates used in the fitting were obtained from inversion recovery experiments.

EPR spectroscopy

Sample concentration was 400 μM and 3 mM for measurement at 9.5 GHz and 275.7 GHz respectively, in 100 mM sodium phosphate buffer, pH 6.8. Measurements at 9.5 GHz were performed at 40 K with a microwave power of 100 nW and modulation amplitude of 0.5 mT. For measurements at 275.7 GHz these parameters were 10 K, 100 nW and 2.4 mT, respectively. The spectra were simulated using EasySpin (32) for frozen solutions.

Modelling studies to determine the freedom of His ring motion in the tri-nuclear copper center (TNC)

PDB 3cg8 (17) was used to study the extent of His ring rotation allowed at the TNC. Using UCSF Chimera (33) software, the $\chi 2$ dihedral angle of the His residues coordinating the copper at the TNC were changed. Applying the conditions

that there are no clashes with the surrounding atoms, the hydrogen bond (Table S3) with the His $N^{\delta 1}$ is kept and the distance between His $N^{\delta 1}$ – Cu(II) is ≤ 0.05 Å to maintain the coordination bond, the range of the allowed value of the $\chi 2$ dihedral angle was determined.

Equations to obtain exchange rates

$$\frac{\sum \text{Cross}}{\sum \text{Dia}} = \frac{I_{ij} + I_{ji}}{I_{ii} + I_{jj}} \ (24) \tag{S2.1}$$

where $\sum$ Cross and $\sum$ Dia is the summation of integral volumes of the cross peaks and diagonal peaks, respectively and,

$$I_{ii} = I_{i0}\frac{-(\lambda_2 - a_{ii})\mathrm{e}^{-\lambda_1\tau_m} + (\lambda_1 - a_{ii})\mathrm{e}^{-\lambda_2\tau_m}}{\lambda_1 - \lambda_2}$$
$$I_{jj} = I_{j0}\frac{-(\lambda_2 - a_{jj})\mathrm{e}^{-\lambda_1\tau_m} + (\lambda_1 - a_{jj})\mathrm{e}^{-\lambda_2\tau_m}}{\lambda_1 - \lambda_2} \tag{S2.2}$$

$$I_{ij} = I_{i0}\frac{a_{ji}\mathrm{e}^{-\lambda_1\tau_m} - a_{ji}\mathrm{e}^{-\lambda_2\tau_m}}{\lambda_1 - \lambda_2}$$
$$I_{ji} = I_{j0}\frac{a_{ij}\mathrm{e}^{-\lambda_1\tau_m} - a_{ij}\mathrm{e}^{-\lambda_2\tau_m}}{\lambda_1 - \lambda_2} \tag{S2.3}$$

$$\lambda_{1,2} = \frac{1}{2}\left\{(a_{ii} + a_{jj}) \pm \sqrt{(a_{ii} - a_{jj})^2 + 4k_{ij}k_{ji}}\right\} \tag{S2.4}$$

$$a_{ii} = R_i + k_{ij};\ a_{jj} = R_j + k_{ji};\ a_{ij} = -k_{ji};\ a_{ji} = -k_{ij}$$

Where I_{ii}, I_{jj} are the intensities of the diagonal peaks, I_{i0}, I_{j0} are the initial diagonal intensities at 0 ms mixing time, I_{ij}, I_{ji} are the intensities of the cross peaks, k_{ij}, k_{ji} are the forward and reverse exchange rates, respectively and R_i, R_j are the spin-lattice relaxation rates of the two sites.

Supporting figures and tables

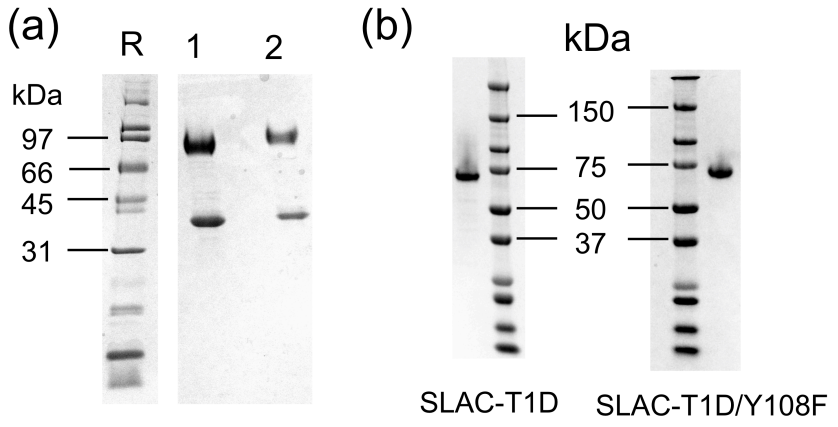

Figure S2.1. *(a) 12.5% SDS PAGE of purified SLAC-T1D. Lane R is the molecular marker with molecular weights in kDa, in lane 1 and 2 are the perdeuterated and fully protonated sample respectively. The samples were heated at 95°C for 30 s before loading on the gel. The detail description is given in the main text; (b) Image of a Bis-Tris precast SDS PAGE gel (ThermoFischer scientific) of purified SLAC-T1D and SLAC-T1D/Y108F without heating.*

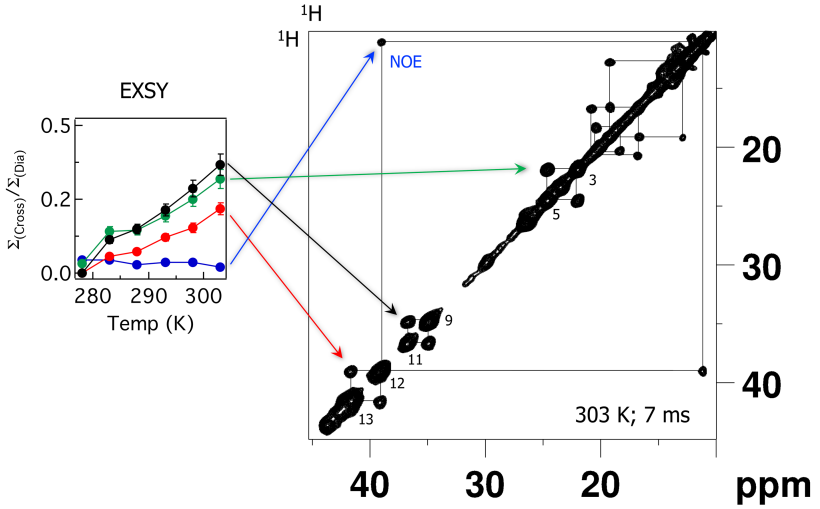

Figure S2.2. *^{1}H-^{1}H EXSY spectra acquired at 303 K and a mixing time of 7 ms. The plot on the left shows the temperature dependence of the integral volume of cross peaks normalized to the integral volume of the diagonal peaks for the resonance pair 3-5 (green), 9-11 (black), 13-12 (red) and 12- resonance at 11 ppm (blue) with the error bars that are the standard error of the mean derived from the duplicate experiments.*

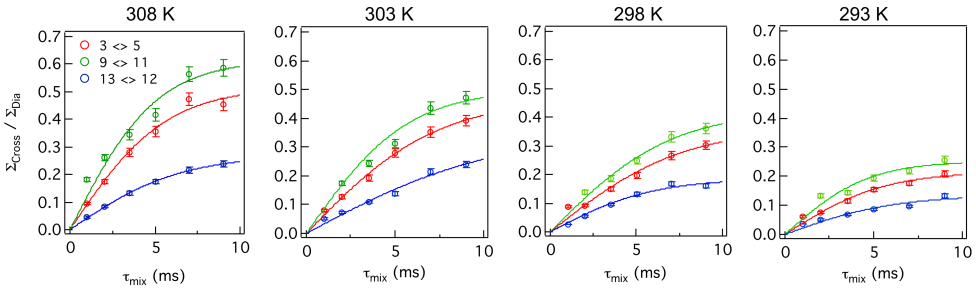

Figure S2.3. *Fits of the intensity profile of normalized cross peak integrals from the resonance pairs of 3-5, 9-11 and 13-12 at different temperatures to equations S2.1 to S2.4. The error bars represent the standard error of the mean derived from the duplicate experiments.*

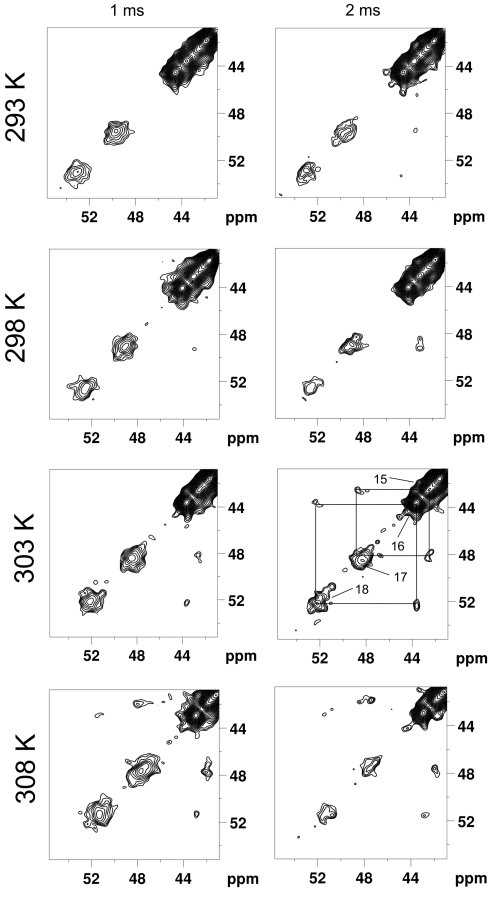

Figure S2.4. *^{1}H-^{1}H EXSY from resonances 17 and 18 at different temperatures and with mixing times of 1 ms and 2 ms. Cross-peaks are marked at 303 K with 2 ms mixing time between the resonance pairs 17-15 and 18-16.*

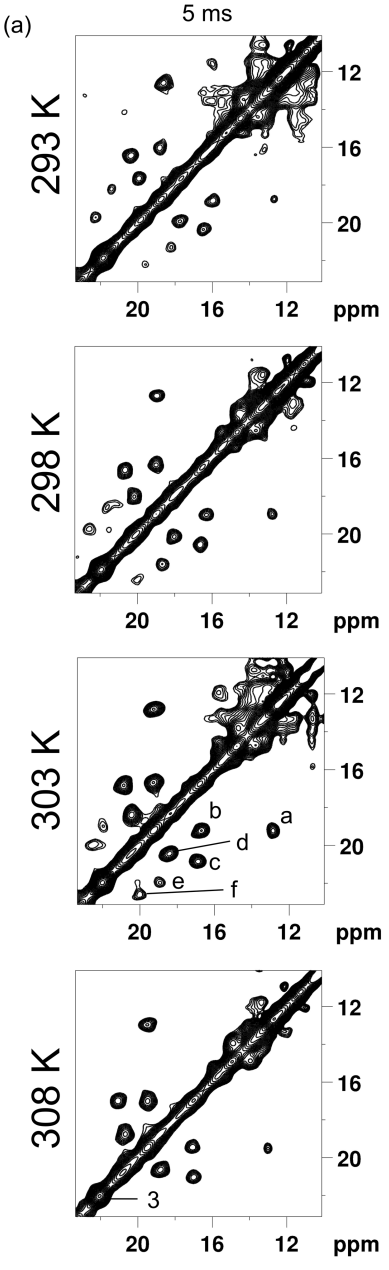

(b)

Cross peak	ppm (293 K)
	Dia 1 to Dia 2
a	18.62 to 12.65
b	18.78 to 16.00
c	20.34 to 16.40
d	19.89 to 17.66
e	21.35 to 18.21
f	22.20 to 19.62

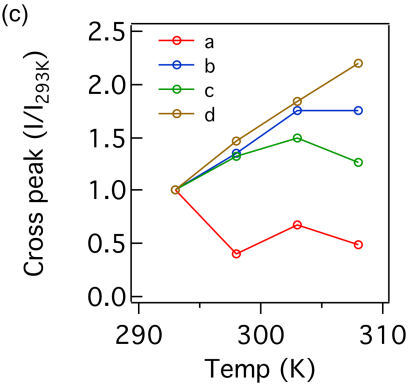

Figure S2.5. *(a) ^{1}H-^{1}H EXSY spectra at different temperatures, showing the region between 10 and 22 ppm. The cross peaks are labelled in the spectrum recorded at 303 K, (b) Chemical shifts of the diagonal peaks having cross peaks and (c) Temperature dependence of the cross-peak integrals of a, b, c and d.*

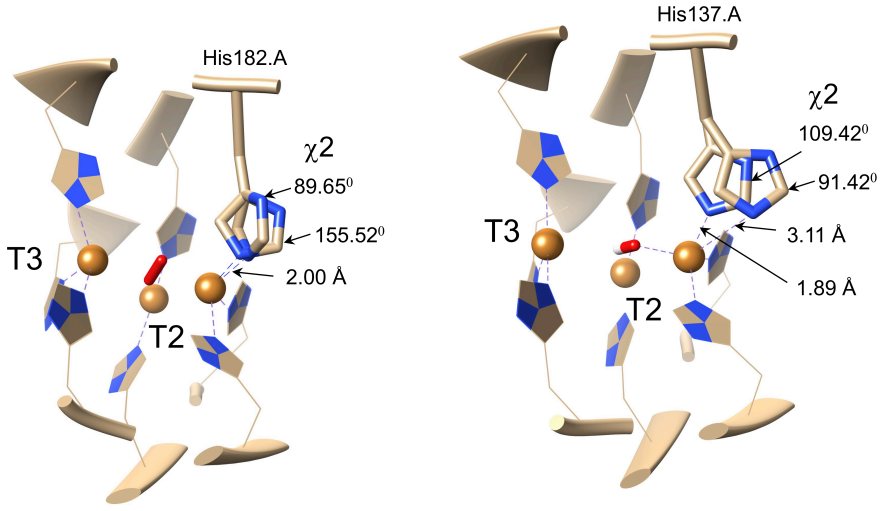

Figure S2.6. *Conformational freedom in TNC histidine ligands. (a) TNC of laccase from Campylobacter jejuni showing two conformations of His182.A (PDB 3zx1, resolution 1.95 Å) (26) due to a change in the χ2 dihedral angle. Both conformers coordinate the copper. (b) TNC of laccase from Thermus thermophilus HB27 (PDB 2xu9 resolution 1.50 Å) (27) showing two conformations for His137A. The χ2 dihedral changes by ~ 20° but the χ1 dihedral change by ~ 140° resulting in the loss of coordination of the copper.*

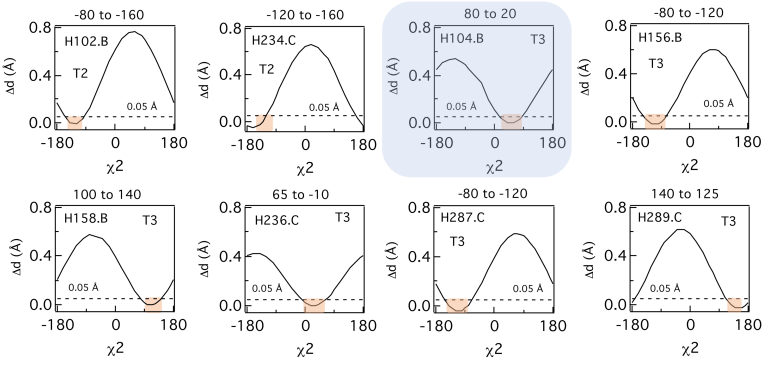

Residue	Original χ2 dihedral angle
His102.B	-114.02
His234.C	-131.47
His104.B	58.70
H156.B	-88.49
H158.B	114.62
H236.C	32.04
H287.C	-82.25
H289.C	127.01

Figure S2.7. *Difference of T3Cu – Nε2 distance from the original crystallographic distance as a function of the χ2 dihedral angle for His ligands (number.chain-ID) from PDB 3cg8 (17) of SLAC. Assuming that the coordination would be lost if the distance were to increase more than 0.05 Å and applying the condition that there are no clashes with the surrounding atoms and the hydrogen bond with the His Nδ1 is maintained, the structure would allow for the χ2 angle to vary between the values given above the graphs and highlighted in the graphs. Nδ1 of His104.B has no hydrogen bond (highlighted graph). The table shows the χ2 angle observed in the structure.*

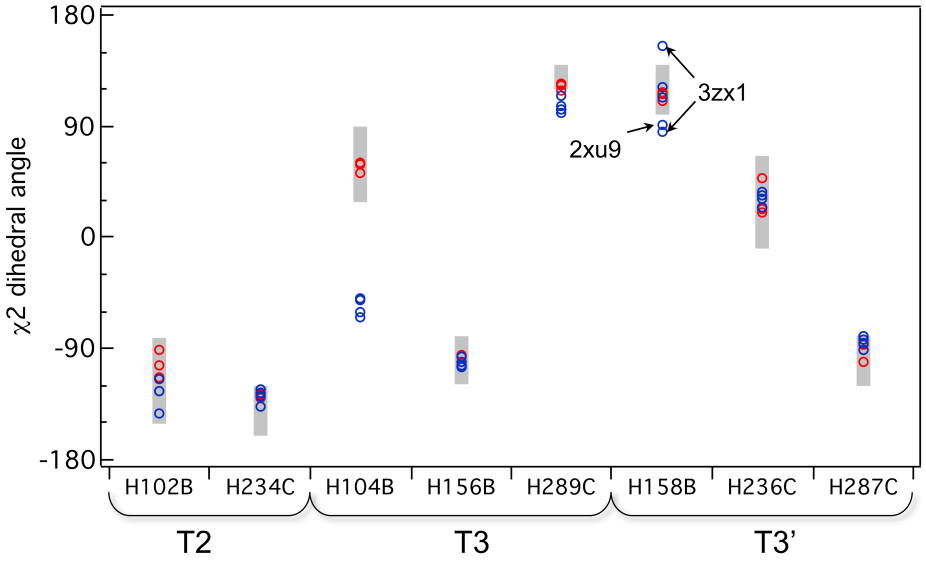

Figure S2.8. *Distribution of the χ2 dihedral angle of the His ligands at the TNC from structures of different prokaryotic laccases. The number and chain ID (residue.number.chain) scheme is adopted from PDB 3cg8, the structure of SLAC from S. coelicolor. Blue and red data points are from the bacterial 3-domain and 2-domain laccases, respectively. The grey bars represent the ranges shown in Figure S2.7. The crystal structures used are 3cg8,(17) 5lhl,(34) 1gsk,(35) 2fqe,(36) 3t9w,(37) 3g5w,(38) 2xu9,(27) and 3zx1(26) for laccases from S. coelicolor, S. griseoflavus, Bacillus subtilis, E. coli, Amycolatopsis sp. ATCC 39116, Nitrosomonas europaea, Thermus thermophilus HB27 and Campylobacter jejuni Cgug11284, respectively. In 3-domain laccases (1gsk, 2fqe, 3g5w, 2xu9 and 3zx1) the Nδ1 atom of H104 coordinates the copper rather than the Nε2 atom in the case of 2-domain laccases. For 3zx1 two χ2 dihedral angles were observed for H158.*

The Python code to extract the information of the χ2 dihedral angle of the histidine ligands from a PDB file can be found in:

https://github.com/rubindg/chi2_dihedral_angle_histidine_copper_protein

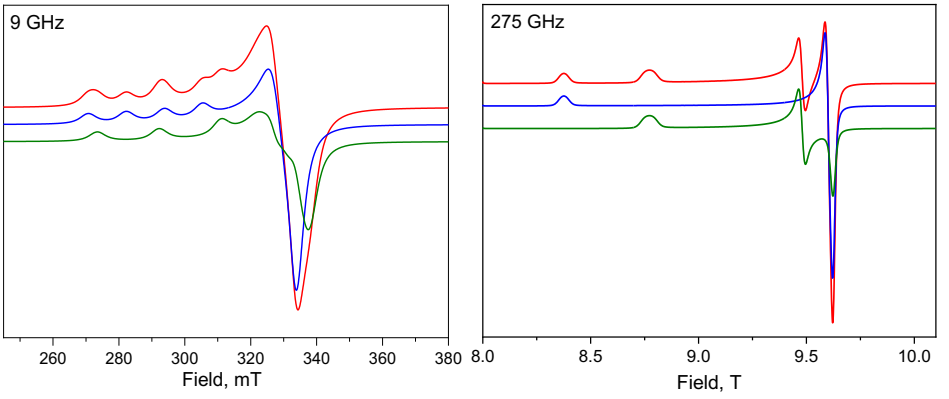

Figure S2.9. *Simulated (red line and Figure 2.3 in the main text) EPR spectra of the resting form of SLAC-T1D (as purified) at microwave frequencies of 9.5 GHz and 275 GHz. The separate contributions of major component 1 (65%) and minor component 2 (35%) to the simulated spectra are shown in blue and green, respectively. The hyperfine interactions of the copper electron spin with the nitrogen nuclei of the copper-coordinating histidine ligands are not considered for the simulations.*

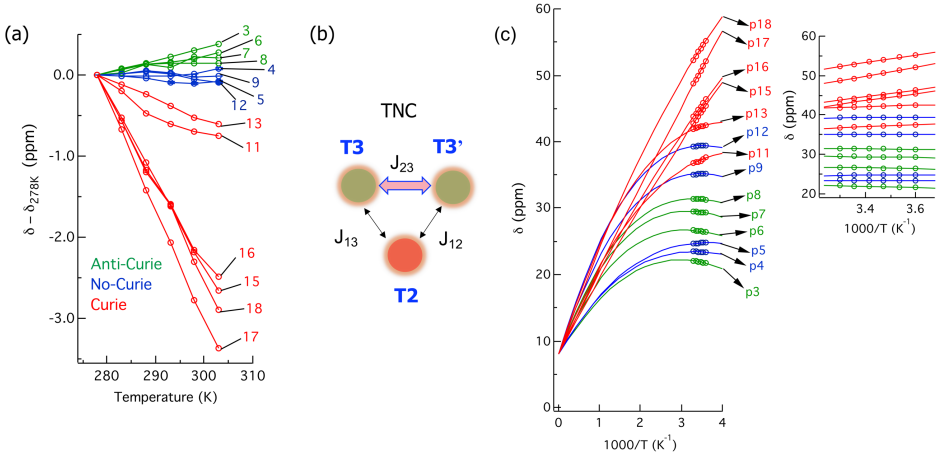

Figure S2.10*. (a) Temperature dependence of the FCS resonances marked as anti-Curie (green), Curie (red) and no-Curie (blue), (b) The tri-nuclear copper center with respective J couplings between different pairs of coppers and (c) Temperature dependence of the paramagnetically shifted resonances. Solid lines shows the simulation based on the J coupling values obtained from Machczynski et al. (2016) (19) The inset shows the zoomed area of the data points highlighting the quality of the simulation over the data points.*

Table S2.1*. Chemical shifts of the paramagnetically shifted resonances (corresponding to Figure 2.1b in the main text) at ^{1}H Larmor frequency of 600 MHz.*

Resonance	Chemical shift in ppm at 288 K
1	17.66
2	19.65
3	21.94
4	23.48
5	24.73
6	26.56
7	29.47
8	31.63
9	35.21
10	36.20
11	37.45
12	39.37
13	42.28
14	41.19
15	44.52
16	45.27
17	50.76
18	54.09

Table S2.2*. Spin-lattice relaxation rates (s^{-1})* as obtained from inversion recovery experiment and used in the fitting in equation S2.1.*

Temp (K)	Spin lattice relaxation (s^{-1})					
	3	***5***	***9***	***11***	***12***	***13***
293	169	509	144	525	180	499
298	225	457	240	464	170	492
303	180	404	241	422	407	566
308	192	486	225	463	210	477

[*] Error is estimated to be ~ ± 5% from duplicate measurements.

Table S2.3. *Residues and atoms that forms the hydrogen bond(s) (H-bond) with Nδ1 of coordinating His ligands at the TNC (obtained from PDB 3cg8). The residue number and chain ID are given. O is the backbone carbonyl oxygen or oxygen from water molecule. His ligands in red are from the T2 site.*

Ligand	Residue forming H-bond
H158.B	E163.B O H158.B O
H236.C	H_2O 676.C O
H287.C	C288.C O
H289.C	H289.C O
H156.B	D157.B O
H104.B	-
H102.B	H_2O 629.B O D113.B O
H234.C	D259.C O

Table S2.4*. Spin Hamiltonian parameters used for the simulation of the experimental EPR spectra of SLAC-T1D. A g-strain of (0.0015 0.0025 0.008) is included for both components.*

Spin Hamiltonian parameters	Major Component 1	Minor Component 2
A_x (MHz)	40	40
A_y (MHz)	50	50
A_z (MHz)	380	590
g_x	2.047	2.047
g_y	2.052	2.078
g_z	2.352	2.246

***Table S2.5**. Estimated PCS contribution to the observed chemical shift using equation 1.11 and the J coupling values of J_{12} = –120 cm^{-1}, J_{13} = –80 cm^{-1} and J_{23} = –150 cm^{-1} (Figure S2.10b).(19) The g-anisotropy for T3 site was assumed to be 0.4 (39) and for the T2 site it was calculated from Table S2.4 for major and minor components. The value of θ was 0°. The protons were modelled using add hydrogen tool in UCSF chimera to get an estimation of the distance to the copper atom using PDB 3cg8.(17, 33) Bold font represents the His coordinating the T2 copper, blue represents the His coordinating T3 site copper and black T3' copper.*

Proton (Hδ1)	PCS_T3 (ppm)	PCS_T3' (ppm)	PCS_T2_Component 1 (ppm)	PCS_T2_Component 2 (ppm)
His102	0.94	0.56	6.23	3.70
His234	0.55	0.84	5.90	3.50
His158	1.30	0.33	1.10	0.66
His236	1.58	0.32	4.50	2.72
His287	1.25	0.50	1.27	0.75
His289	0.60	1.58	1.23	0.73
His156	0.60	1.57	1.57	0.93
His104	0.37	1.62	5.56	3.30

***Table S2.6**. EPR parameters of the T2 site in g_z-region of multicopper oxidases from different organisms around pH 7. wt, T1D and T1Hg refer to wild-type, T1 copper depleted and T1 copper replaced by Hg, respectively.*

Protein	Organism	g_z	A_z (MHz)	Reference
Laccase-wt	*Trametes hirsuta*	2.260	557	(40)
Laccase-wt	*Trametes ochracea*	2.240	581	(40)
Laccase-wt	*Cerrena maxima*	2.240	581	(40)
Laccase-wt	*Coriolopsis fulvocinera*	2.230	582	(40)
Laccase-wt	*Rhus vernicefera*	2.237	599	(41)
Ceruloplasmin	Human	2.270	524	(42)
Fet3p-T1D	*Saccharomyces cerevisiae*	2.243	570	(43, 44)
Laccase-T1Hg	*Rhus vernicefera*	2.246	587	(45)
Laccase-wt	*Pleurotus ostreatus* (POXC)	2.233	587	(46)
Laccase-wt	*Rigidoporus lignosus* (POXB)	2.241	577	(46)

2.5 References

1. Mano, N., and A. de Poulpiquet. 2017. O_2 Reduction in Enzymatic Biofuel Cells. *Chem. Rev.*
2. Solomon, E.I., A.J. Augustine, and J. Yoon. 2008. O_2 Reduction to H_2O by the multicopper oxidases. *Dalton Trans.* 3921–3932.
3. Heppner, D.E., C.H. Kjaergaard, and E.I. Solomon. 2014. Mechanism of the Reduction of the Native Intermediate in the Multicopper Oxidases: Insights into Rapid Intramolecular Electron Transfer in Turnover. *J. Am. Chem. Soc.* 136:17788–17801.
4. Lee, S.-K., S.D. George, W.E. Antholine, B. Hedman, K.O. Hodgson, and E.I. Solomon. 2002. Nature of the Intermediate Formed in the Reduction of O_2 to H_2O at the Trinuclear Copper Cluster Active Site in Native Laccase. *J. Am. Chem. Soc.* 124:6180–6193.
5. Palmer, A.E., S.K. Lee, and E.I. Solomon. 2001. Decay of the Peroxide Intermediate in Laccase: Reductive Cleavage of the O−O Bond. *J. Am. Chem. Soc.* 123:6591–6599.
6. Machczynski, M.C., E. Vijgenboom, B. Samyn, and G.W. Canters. 2004. Characterization of SLAC: A small laccase from *Streptomyces coelicolor* with unprecedented activity. *Protein Science.* 13:2388–2397.
7. Tepper, A.W.J.W., S. Milikisyants, S. Sottini, E. Vijgenboom, E.J.J. Groenen, and G.W. Canters. 2009. Identification of a Radical Intermediate in the Enzymatic Reduction of Oxygen by a Small Laccase. *Journal of the American Chemical Society*. 131:11680–11682.
8. Gupta, A., I. Nederlof, S. Sottini, A.W.J.W. Tepper, E.J.J. Groenen, E.A.J. Thomassen, and G.W. Canters. 2012. Involvement of Tyr108 in the Enzyme Mechanism of the Small Laccase from *Streptomyces coelicolor*. *Journal of the American Chemical Society*. 134:18213–18216.
9. Wang, J., K. Wang, F.-B. Wang, and X.-H. Xia. 2014. Bioinspired copper catalyst effective for both reduction and evolution of oxygen. *Nat Commun*. 5:5285.
10. van Dijk, B., J.P. Hofmann, and D.G.H. Hetterscheid. 2018. Pinpointing the active species of the Cu(DAT) catalyzed oxygen reduction reaction. *Phys. Chem. Chem. Phys.* 20:19625–19634.
11. Langerman, M., and D.G.H. Hetterscheid. 2019. Fast Oxygen Reduction Catalyzed by a Copper(II) Tris(2-pyridylmethyl)amine Complex through a Stepwise Mechanism. *Angewandte Chemie*. 131:13108–13112.
12. Thorum, M.S., J. Yadav, and A.A. Gewirth. 2009. Oxygen Reduction Activity of a Copper Complex of 3,5-Diamino-1,2,4-triazole Supported on Carbon Black. *Angewandte Chemie International Edition*. 48:165–167.
13. Brookes, J.C. 2017. Quantum effects in biology: golden rule in enzymes, olfaction, photosynthesis and magnetodetection. *Proceedings of the Royal Society A: Mathematical, Physical and Engineering Science*. 473:20160822.
14. Dorner, R., J. Goold, L. Heaney, T. Farrow, and V. Vedral. 2012. Effects of quantum coherence in metalloprotein electron transfer. *Phys. Rev. E*. 86:031922.
15. Fröhlich, H. 1968. Long-range coherence and energy storage in biological systems. *Int. J. Quantum Chem*. 2:641–649.
16. Lloyd, S. 2011. Quantum coherence in biological systems. *J. Phys.: Conf. Ser.* 302:012037.
17. Skálová, T., J. Dohnálek, L.H. Østergaard, P.R. Østergaard, P. Kolenko, J. Dušková, A. Štěpánková, and J. Hašek. 2009. The Structure of the Small Laccase from *Streptomyces coelicolor* Reveals a Link between Laccases and Nitrite Reductases. *Journal of Molecular Biology*. 385:1165–1178.
18. Bertini, I., C. Luchinat, G. Parigi, and R. Pierattelli. 2005. NMR Spectroscopy of Paramagnetic Metalloproteins. *ChemBioChem*. 6:1536–1549.
19. Machczynski, M.C., and J.T. Babicz. 2016. Correlating the structures and activities of the resting oxidized and native intermediate states of a small laccase by paramagnetic NMR. *Journal of Inorganic Biochemistry*. 159:62–69.
20. Bertini, I., C. Luchinat, G. Parigi, and E. Ravera. 2017. NMR of paramagnetic molecules: applications to metallobiomolecules and models. Second edition. Amsterdam: Elsevier.
21. Bertini, I., C. Luchinat, and G. Parigi. 2002. Magnetic susceptibility in paramagnetic NMR. *Progress in Nuclear Magnetic Resonance Spectroscopy*. 40:249–273.
22. Bertini, I., C. Luchinat, G. Parigi, and R. Pierattelli. 2008. Perspectives in paramagnetic NMR of metalloproteins. *Dalton Transactions*. 0:3782–3790.

23. Jeener, J., B.H. Meier, P. Bachmann, and R.R. Ernst. 1979. Investigation of exchange processes by two-dimensional NMR spectroscopy. *J. Chem. Phys.* 71:4546–4553.
24. Farrow, N.A., O. Zhang, J.D. Forman-Kay, and L.E. Kay. 1994. A heteronuclear correlation experiment for simultaneous determination of ^{15}N longitudinal decay and chemical exchange rates of systems in slow equilibrium. *J Biomol NMR*. 4:727–734.
25. Zaballa, M.-E., L. Ziegler, D.J. Kosman, and A.J. Vila. 2010. NMR Study of the Exchange Coupling in the Trinuclear Cluster of the Multicopper Oxidase Fet3p. *J. Am. Chem. Soc.* 132:11191–11196.
26. Silva, C.S., P. Durão, A. Fillat, P.F. Lindley, L.O. Martins, and I. Bento. 2012. Crystal structure of the multicopper oxidase from the pathogenic bacterium *Campylobacter jejuni* CGUG11284: characterization of a metallo-oxidase. *Metallomics*. 4:37–47.
27. Serrano-Posada, H., S. Centeno-Leija, S.P. Rojas-Trejo, C. Rodríguez-Almazán, V. Stojanoff, and E. Rudiño-Piñera. 2015. X-ray-induced catalytic active-site reduction of a multicopper oxidase: structural insights into the proton-relay mechanism and O_2-reduction states. *Acta Cryst D*. 71:2396–2411.
28. van Gastel, M., J.W.A. Coremans, H. Sommerdijk, M.C. van Hemert, and E.J.J. Groenen. 2002. An ab Initio Quantum-Chemical Study of the Blue-Copper Site of Azurin. *J. Am. Chem. Soc.* 124:2035–2041.
29. Hu, F., W. Luo, and M. Hong. 2010. Mechanisms of Proton Conduction and Gating in Influenza M2 Proton Channels from Solid-State NMR. *Science*. 330:505–508.
30. Hass, M.A.S., D.F. Hansen, H.E.M. Christensen, J.J. Led, and L.E. Kay. 2008. Characterization of Conformational Exchange of a Histidine Side Chain: Protonation, Rotamerization, and Tautomerization of His61 in Plastocyanin from *Anabaena variabilis*. *J. Am. Chem. Soc.* 130:8460–8470.
31. Perrin, C.L., and T.J. Dwyer. 1990. Application of two-dimensional NMR to kinetics of chemical exchange. *Chem. Rev.* 90:935–967.
32. Stoll, S., and A. Schweiger. 2006. EasySpin, a comprehensive software package for spectral simulation and analysis in EPR. *Journal of Magnetic Resonance*. 178:42–55.
33. Pettersen, E.F., T.D. Goddard, C.C. Huang, G.S. Couch, D.M. Greenblatt, E.C. Meng, and T.E. Ferrin. 2004. UCSF Chimera—A visualization system for exploratory research and analysis. *Journal of Computational Chemistry*. 25:1605–1612.
34. Gabdulkhakov, A., I. Kolyadenko, O. Kostareva, A. Mikhaylina, P. Oliveira, P. Tamagnini, A. Lisov, and S. Tishchenko. 2019. Investigations of Accessibility of T2/T3 Copper Center of Two-Domain Laccase from *Streptomyces griseoflavus* Ac-993. *International Journal of Molecular Sciences*. 20:3184.
35. Enguita, F.J., L.O. Martins, A.O. Henriques, and M.A. Carrondo. 2003. Crystal Structure of a Bacterial Endospore Coat Component a laccase with enhanced thermostability properties. *J. Biol. Chem.* 278:19416–19425.
36. Li, X., Z. Wei, M. Zhang, X. Peng, G. Yu, M. Teng, and W. Gong. 2007. Crystal structures of *E. coli* laccase CueO at different copper concentrations. *Biochemical and Biophysical Research Communications*. 354:21–26.
37. Majumdar, S., T. Lukk, J.O. Solbiati, S. Bauer, S.K. Nair, J.E. Cronan, and J.A. Gerlt. 2014. Roles of Small Laccases from Streptomyces in Lignin Degradation. *Biochemistry*. 53:4047–4058.
38. Lawton, T.J., L.A. Sayavedra-Soto, D.J. Arp, and A.C. Rosenzweig. 2009. Crystal Structure of a Two-domain Multicopper Oxidase implications for the evolution of multicopper blue proteins. *J. Biol. Chem.* 284:10174–10180.
39. Tepper, A.W.J.W., L. Bubacco, and G.W. Canters. 2006. Paramagnetic Properties of the Halide-Bound Derivatives of Oxidised Tyrosinase Investigated by ^1H NMR Spectroscopy. *Chem. Eur. J.* 12:7668–7675.
40. Shleev, S.V., O.V. Morozova, O.V. Nikitina, E.S. Gorshina, T.V. Rusinova, V.A. Serezhenkov, D.S. Burbaev, I.G. Gazaryan, and A.I. Yaropolov. 2004. Comparison of physico-chemical characteristics of four laccases from different basidiomycetes. *Biochimie*. 86:693–703.
41. Malmström, B.G., B. Reinhammar, and T. Vänngård. 1970. The state of copper in stellacyanin and laccase from the lacquer tree *Rhus vernicifera*. *Biochimica et Biophysica Acta (BBA) - Bioenergetics*. 205:48–57.

42. Dawson, J.H., D.M. Dooley, and H.B. Gray. 1978. Coordination environment and fluoride binding of type 2 copper in the blue copper oxidase ceruloplasmin. *PNAS*. 75:4078–4081.
43. Augustine, A.J., L. Quintanar, C.S. Stoj, D.J. Kosman, and E.I. Solomon. 2007. Spectroscopic and Kinetic Studies of Perturbed Trinuclear Copper Clusters: The Role of Protons in Reductive Cleavage of the O−O Bond in the Multicopper Oxidase Fet3p. *J. Am. Chem. Soc.* 129:13118–13126.
44. Palmer, A.E., L. Quintanar, S. Severance, T.-P. Wang, D.J. Kosman, and E.I. Solomon. 2002. Spectroscopic Characterization and O_2 Reactivity of the Trinuclear Cu Cluster of Mutants of the Multicopper Oxidase Fet3p. *Biochemistry*. 41:6438–6448.
45. Tamilarasan, R., and D.R. McMillin. 1989. Spectroscopic studies of the type 2 and type 3 copper centres in the mercury derivative of laccase. *Biochemical Journal*. 263:425–429.
46. Garzillo, A.M., M.C. Colao, V. Buonocore, R. Oliva, L. Falcigno, M. Saviano, A.M. Santoro, R. Zappala, R.P. Bonomo, C. Bianco, P. Giardina, G. Palmieri, and G. Sannia. 2001. Structural and Kinetic Characterization of Native Laccases from *Pleurotus ostreatus, Rigidoporus lignosus*, and *Trametes trogii*. *J Protein Chem*. 20:191–201.